

1 **Supplement of**

2 **Modeling of the chemistry in oxidation flow reactors with high NO injection**

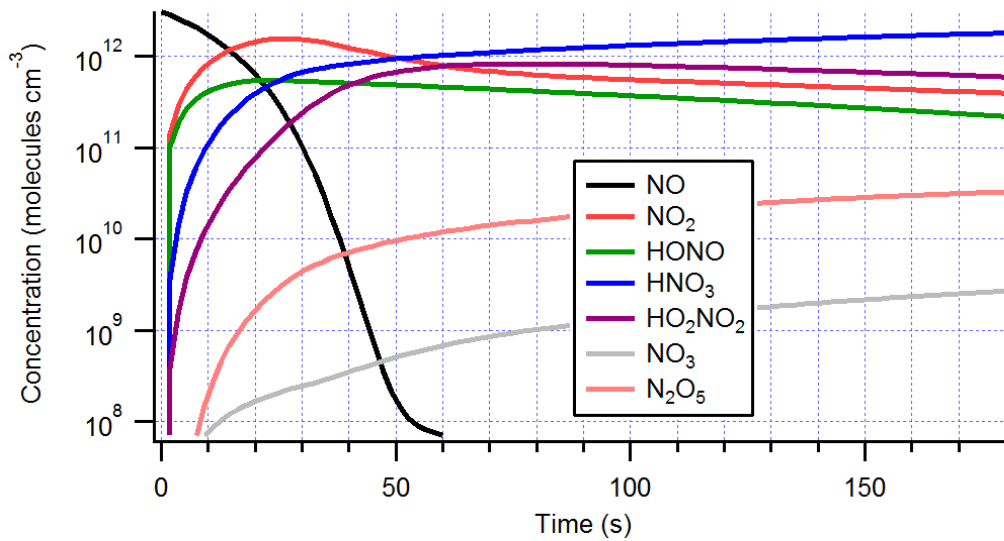
3 Zhe Peng^{1,2} and Jose L. Jimenez^{1,2}

4 ¹Cooperative Institute for Research in Environmental Sciences, University of Colorado, Boulder, CO 80309, USA

5 ²Department of Chemistry and Biochemistry, University of Colorado, Boulder, CO 80309, USA

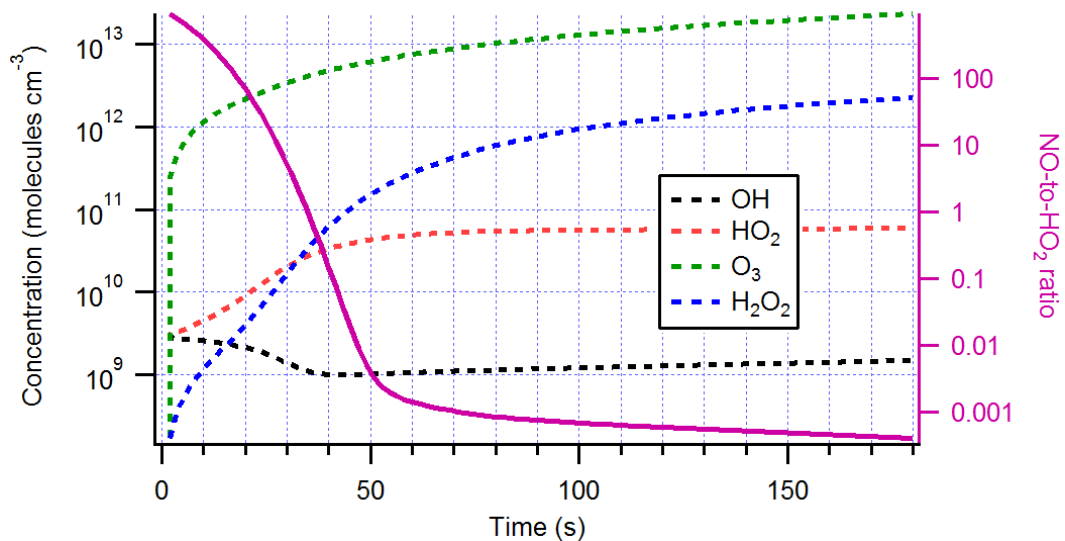
6 Correspondence to: J.L. Jimenez (jose.jimenez@colorado.edu)

7



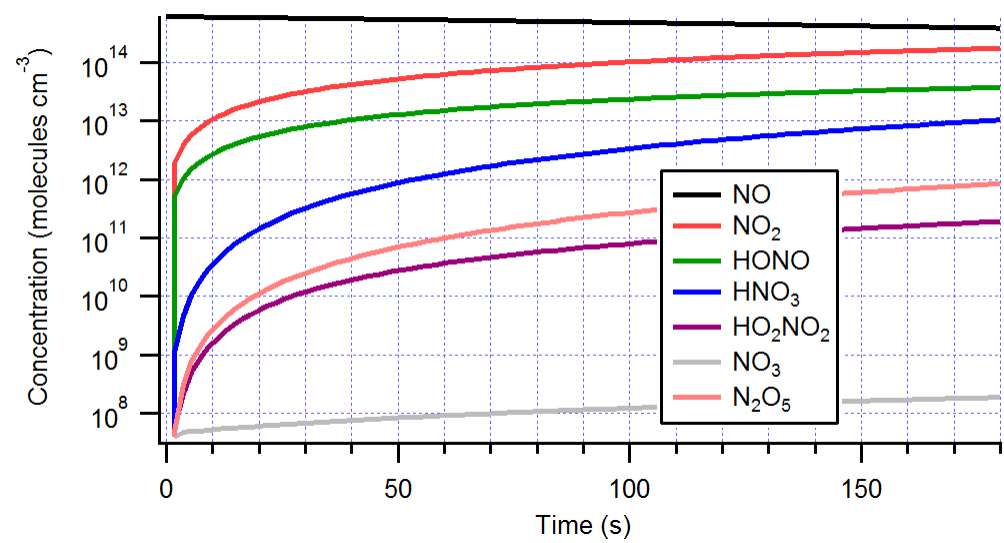
8
9

(a) OFR185-iNO (150 ppb NO)



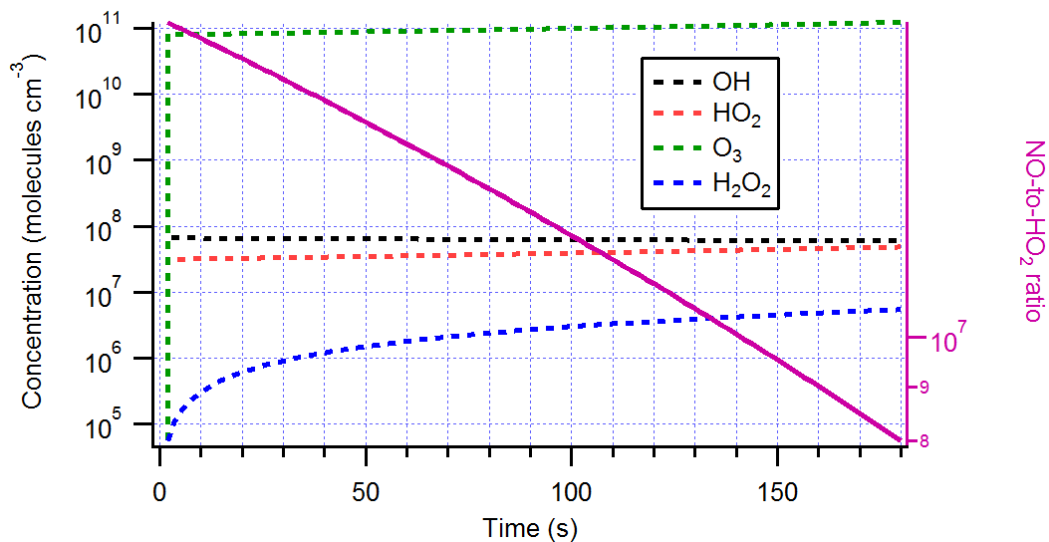
10
11

(b) OFR185-iNO (150 ppb NO)



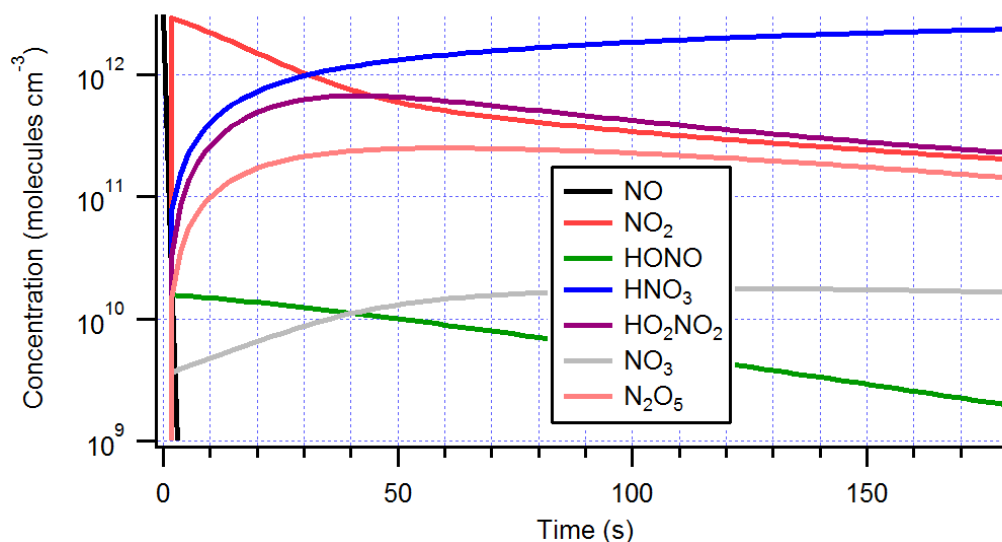
12
13

(c) OFR185-iNO (30 ppm NO)



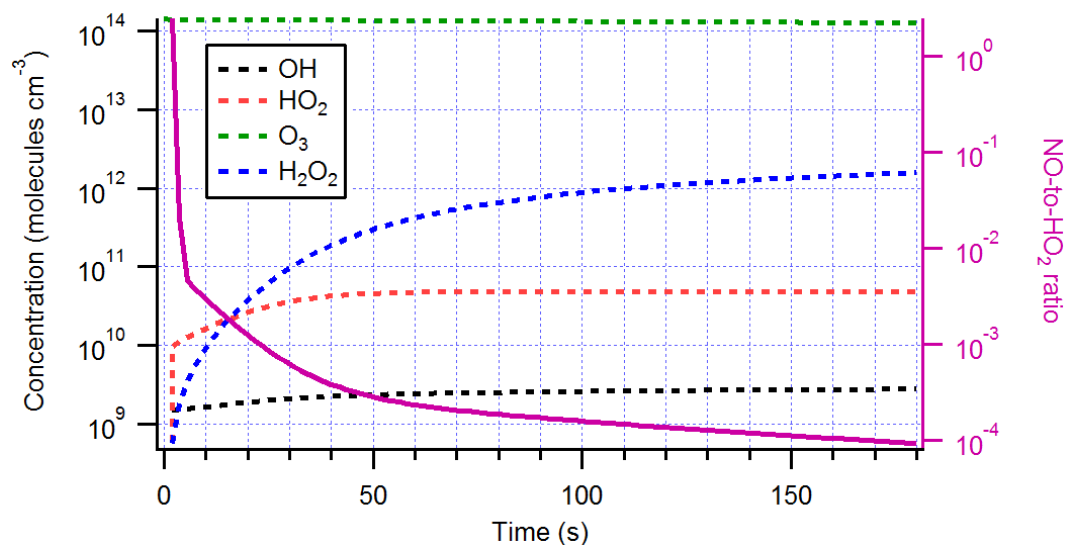
14
15

(d) OFR185-iNO (30 ppm NO)



16
17

(e) OFR254-iNO (150 ppb NO)

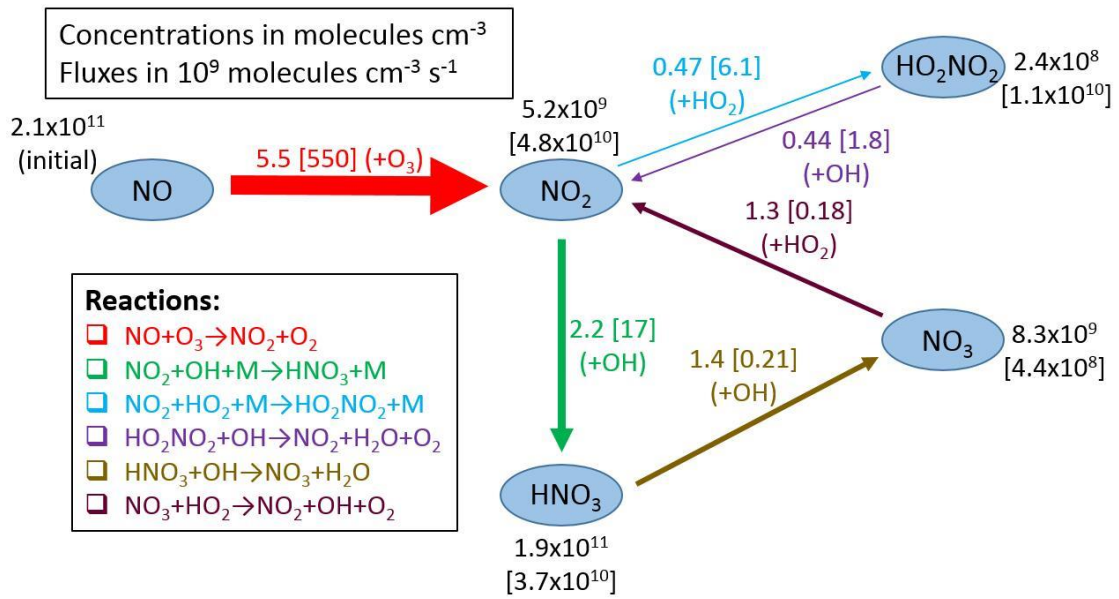


18
19

(f) OFR254-iNO (150 ppb NO)

20 **Figure S1.** Concentrations of (a, c, e) several NO_y species and (b, d, f) OH, HO₂, O₃, and H₂O₂ and ratio of

- 21 NO concentration to that of HO₂ as a function of reaction time in the cases shown in Fig. 1 (OFR185-iNO
22 with 150 ppb initial NO, OFR185-iNO with 30 ppm initial NO, and OFR254-iNO with 150 ppb initial NO).

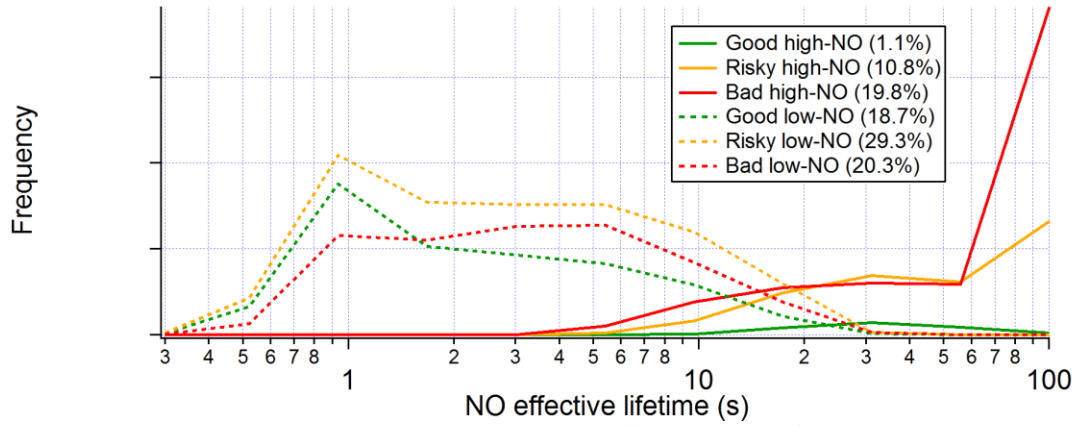


OFR254-7-iNO

(H₂O=1.5%, UV at 254 nm=5x10¹⁵ photons $\text{cm}^{-2} \text{ s}^{-1}$, OHR_{ext}=10 s⁻¹, NOⁱⁿ=10 ppb)

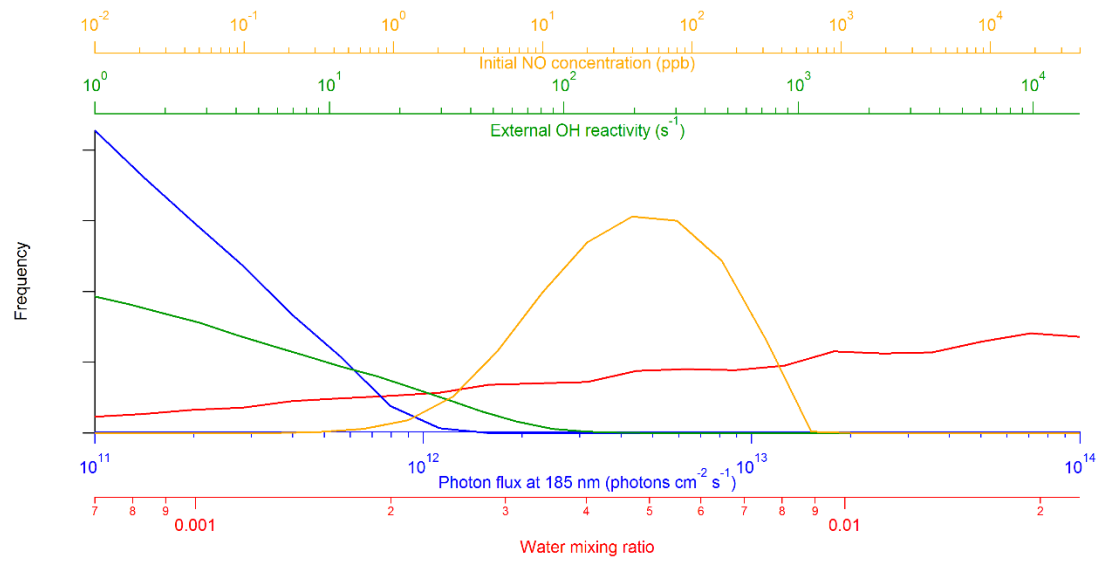
23
24
25

Figure S2. Same format as Fig. 1b, but at a lower initial NO level.



26
27
28

Figure S3. Frequency occurrence distributions of good/risky/bad high/low-NO conditions over NO effective lifetime for OFR185-iNO.

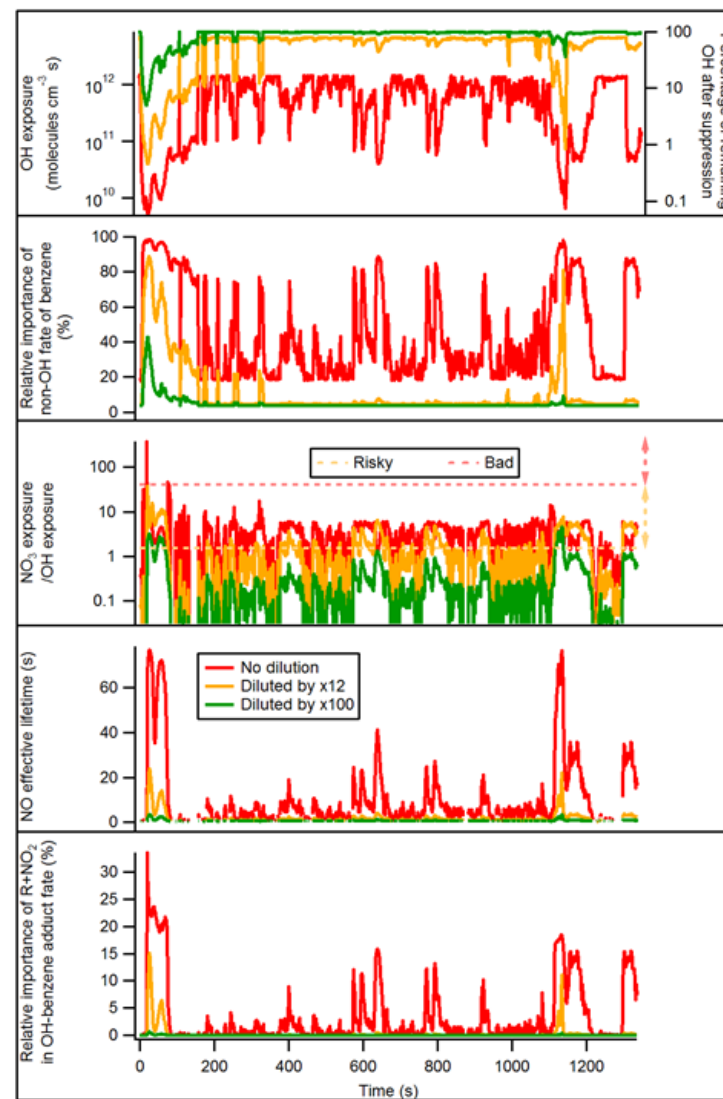
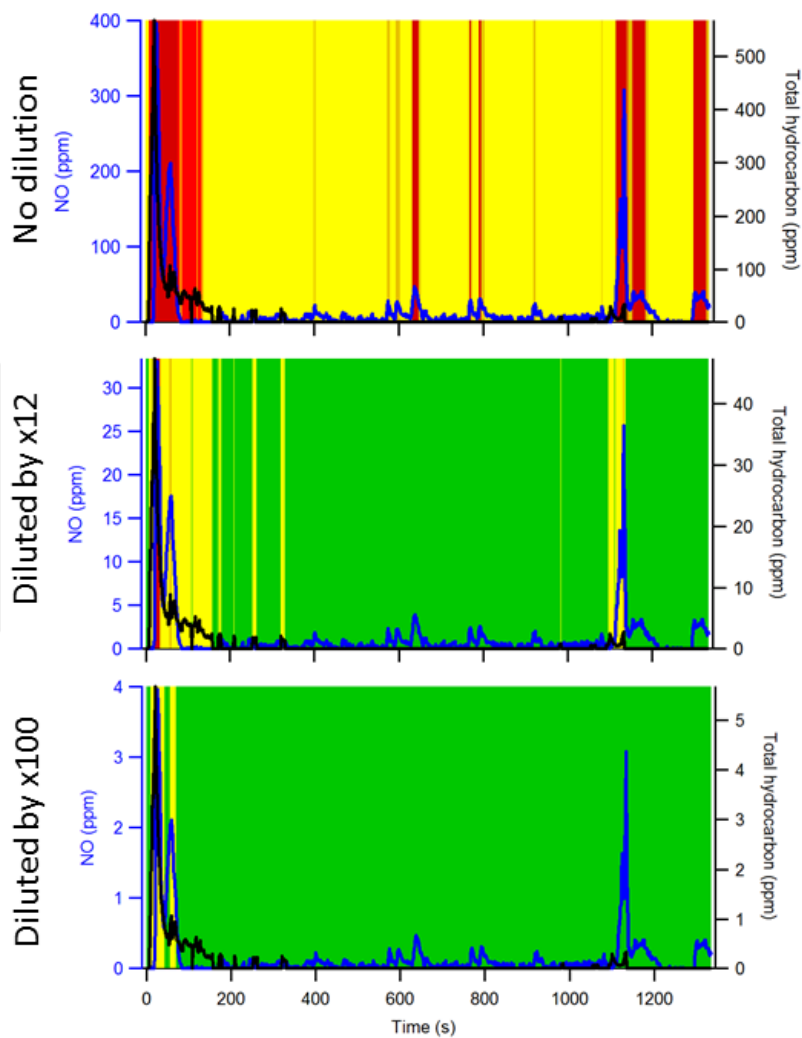
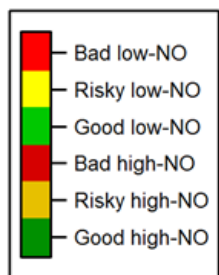


29

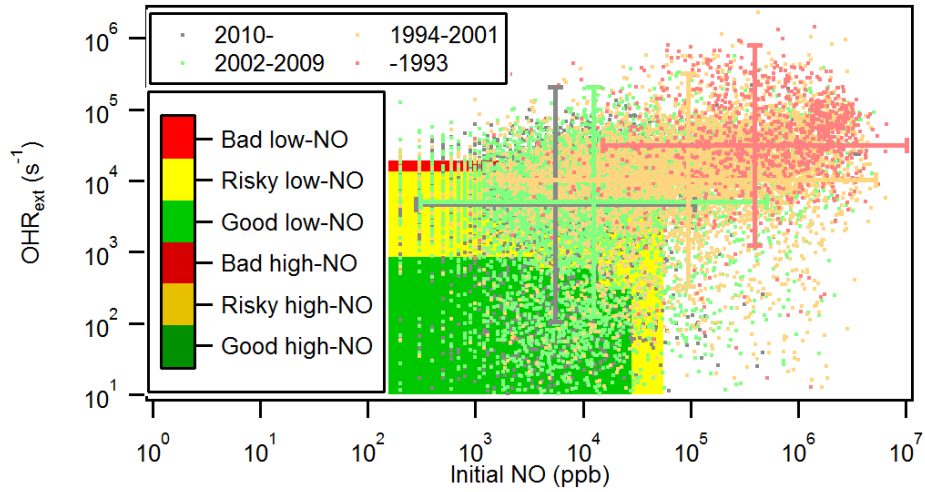
30 **Figure S4.** Frequency occurrence distributions of good high-NO conditions over physical inputs for
 31 OFR185-iNO.

32

33



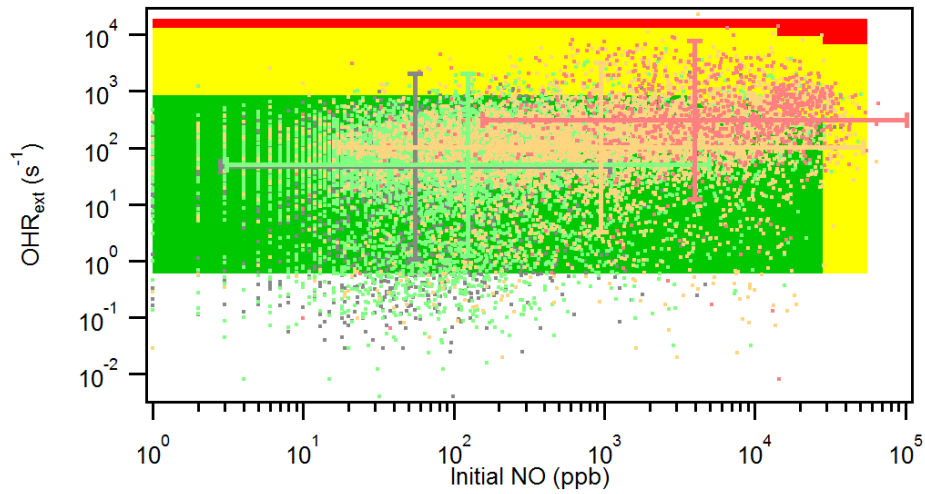
35 **Figure S5.** Same as Fig. 7, but for the entire experiment (~1300 s).
36



37

38

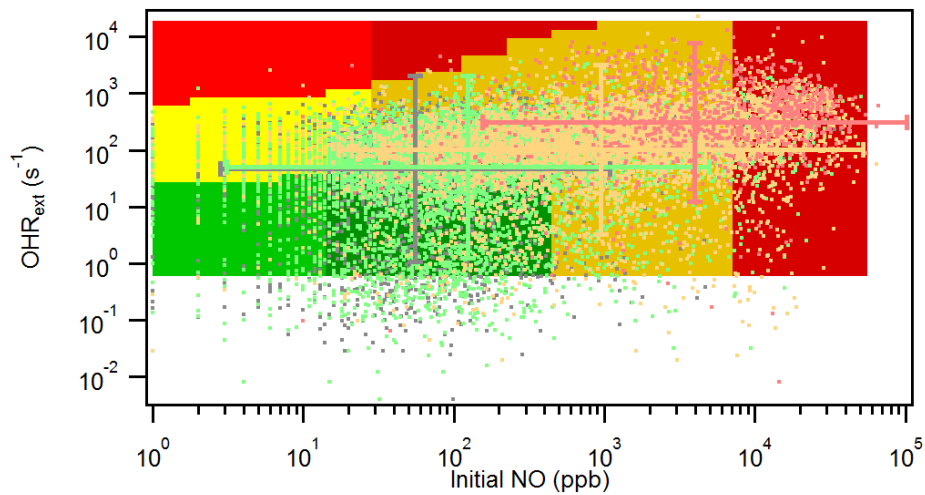
(a) Gasoline vehicles, no dilution (background: Case HH)



39

40

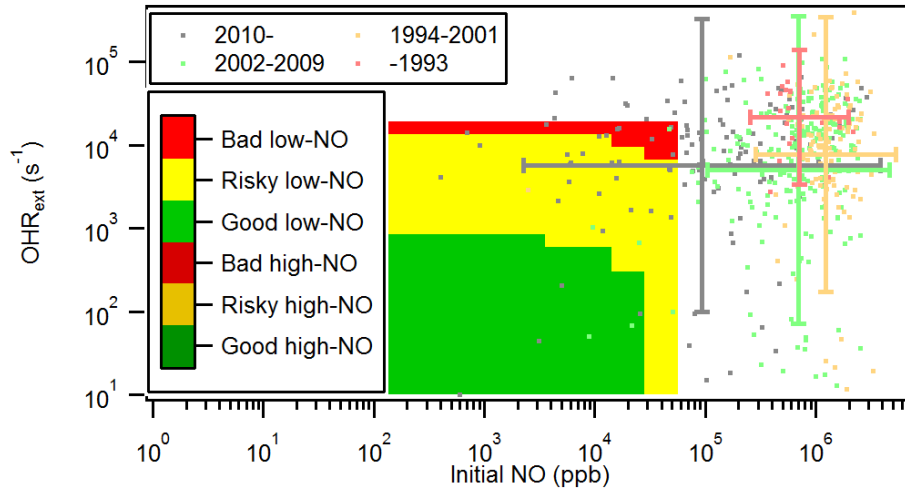
(b) Gasoline vehicles, dilution by a factor of 100 (background: Case HH)



41

42

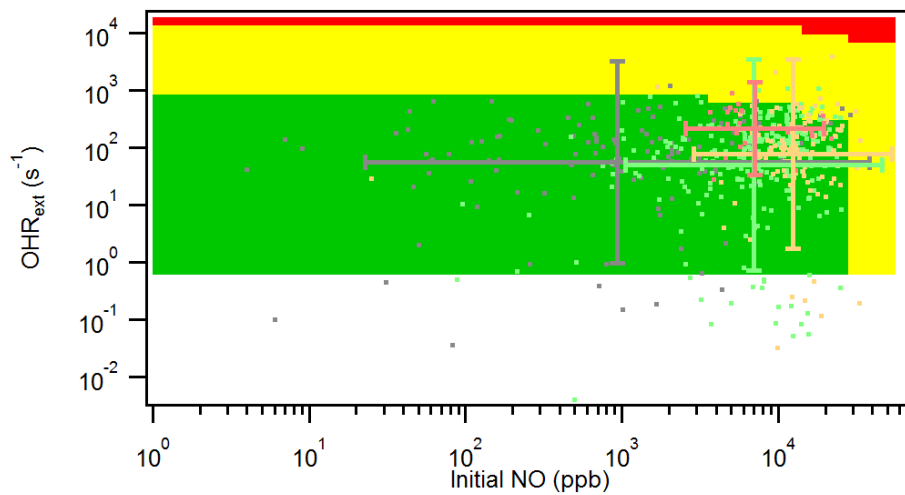
(c) Gasoline vehicles, dilution by a factor of 100 (background: Case HL)



43

44

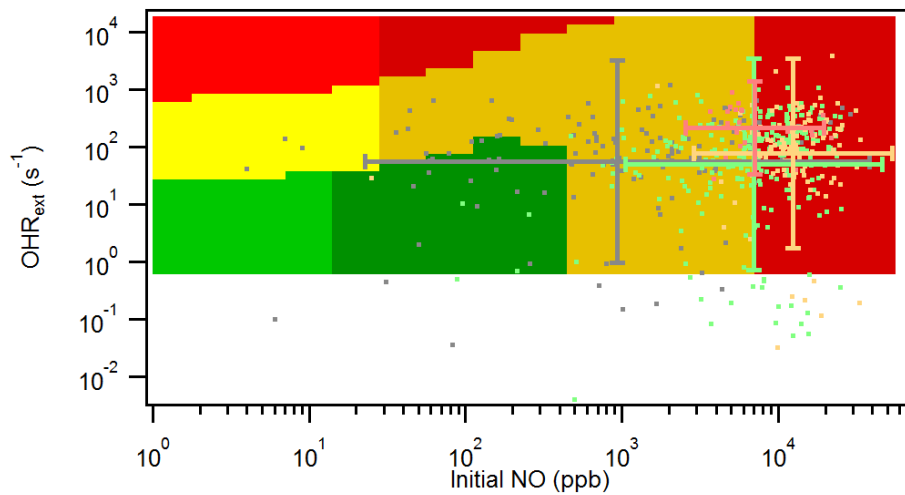
(d) Diesel vehicles, no dilution (background: Case HH)



45

46

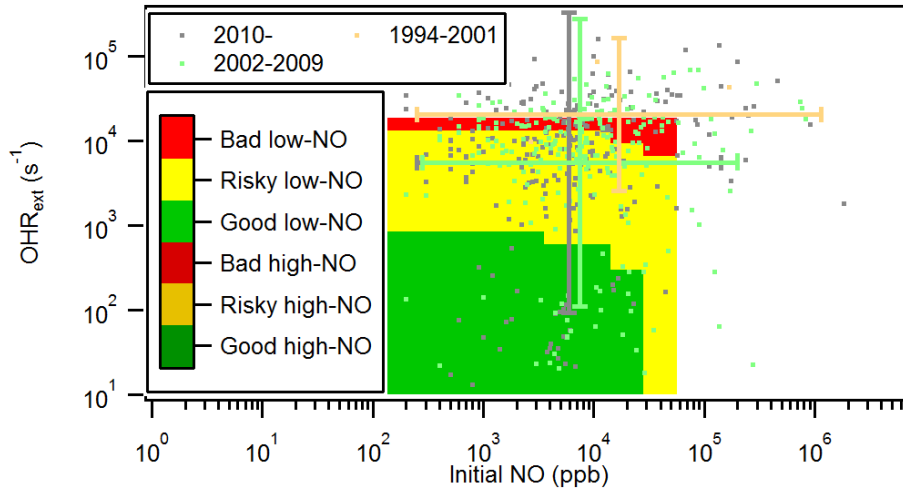
(e) Diesel vehicles, dilution by a factor of 100 (background: Case HH)



47

48

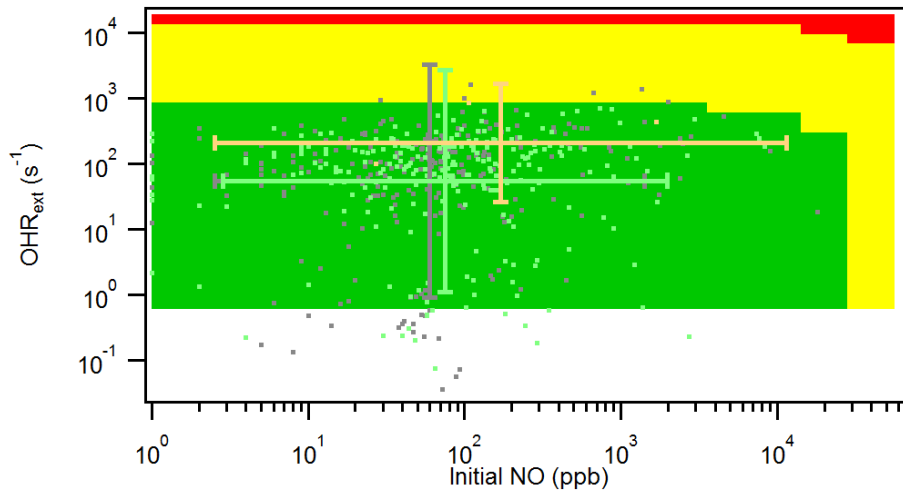
(f) Diesel vehicles, dilution by a factor of 100 (background: Case HL)



49

50

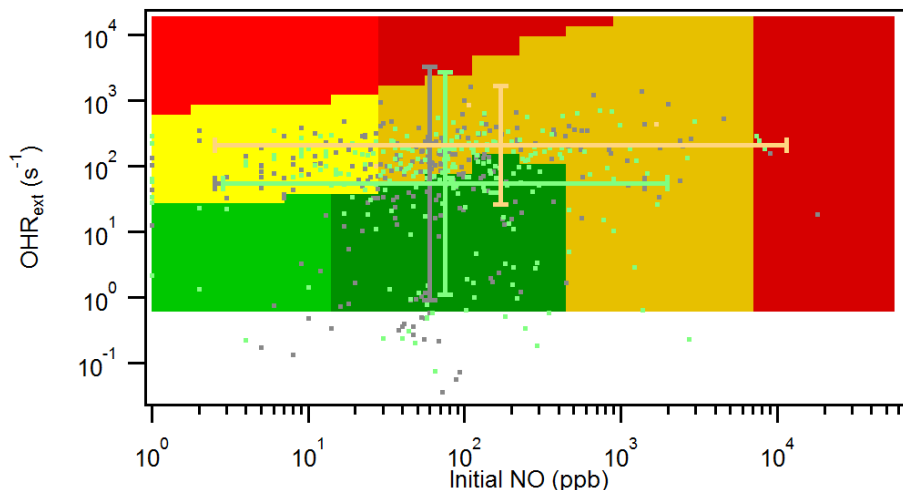
(g) Hybrid vehicles, no dilution (background: Case HH)



51

52

(h) Hybrid vehicles, dilution by a factor of 100 (background: Case HH)



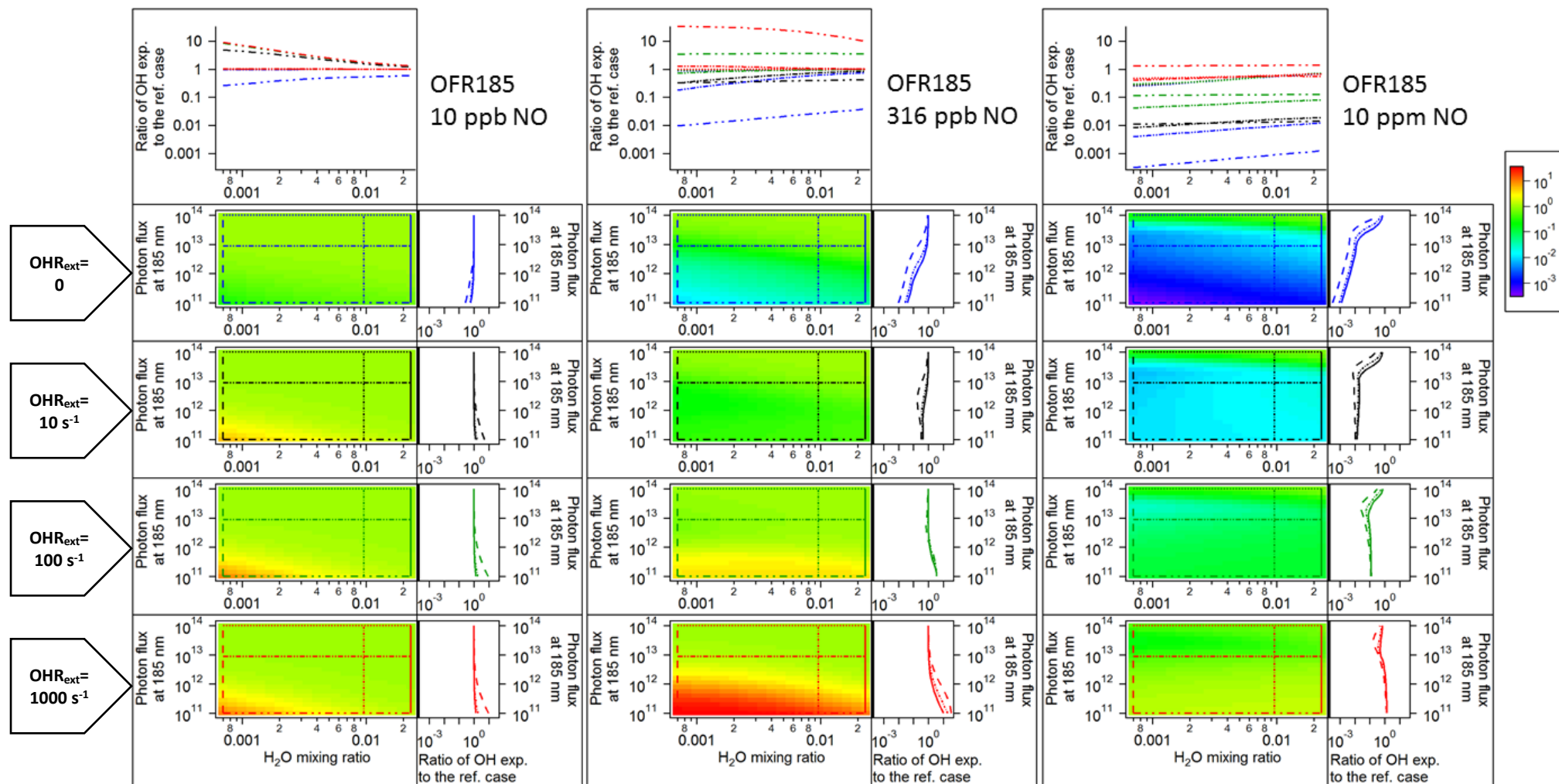
53

54

(i) Hybrid vehicles, dilution by a factor of 100 (background: Case HL)

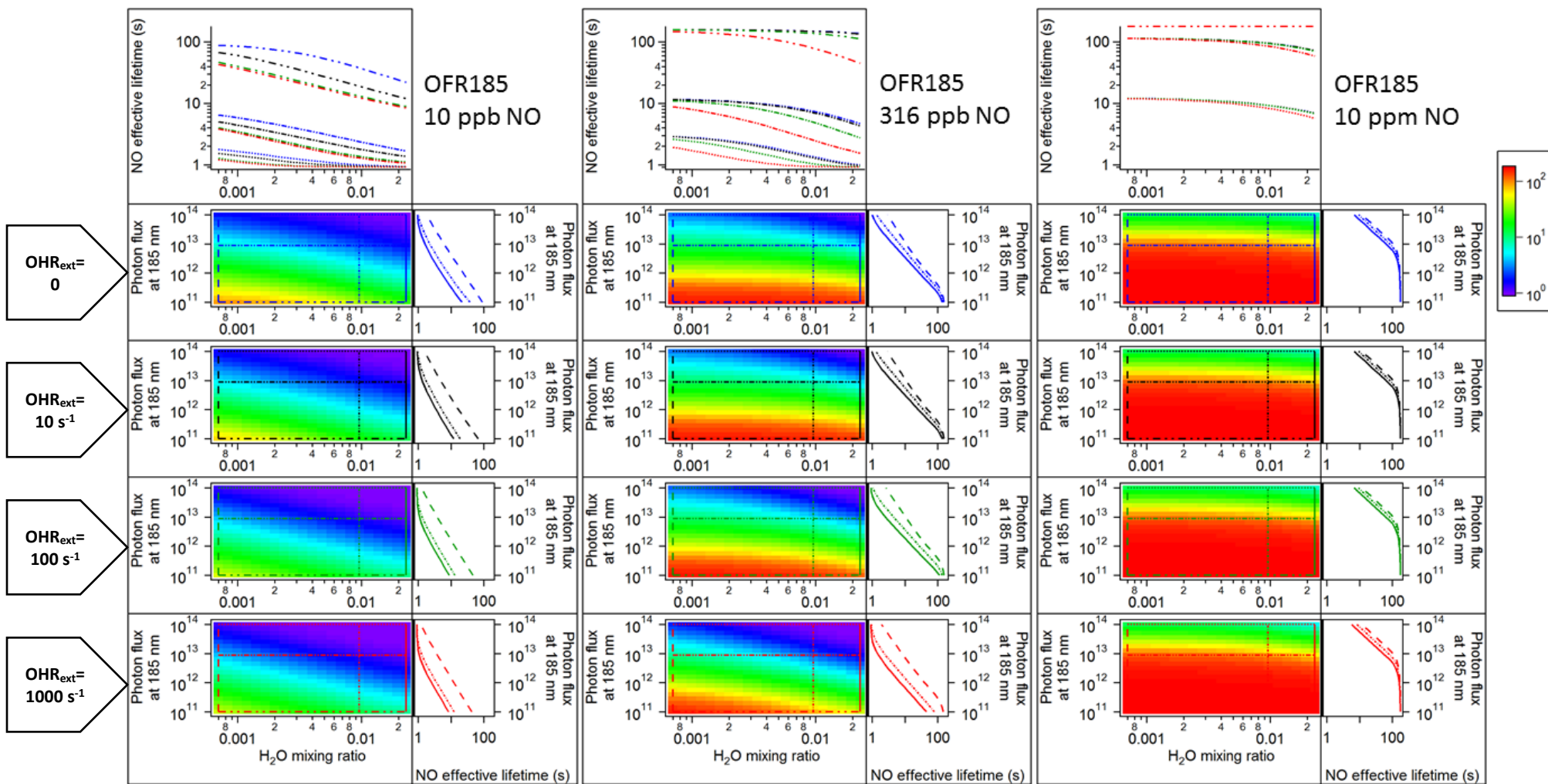
55 **Figure S6.** Similar format as Fig. 9, but without the points for the test of Karjalainen et al. (2016) and with
 56 the scatter points of emissions of individual vehicles measured by Bishop and Stedman (2013). In addition
 57 to (a–c) the scatter points of emissions of gasoline vehicles, those of (d–f) diesel and (g–i) hybrid vehicles
 58 measured by Bishop and Stedman (2013) are also shown.

59



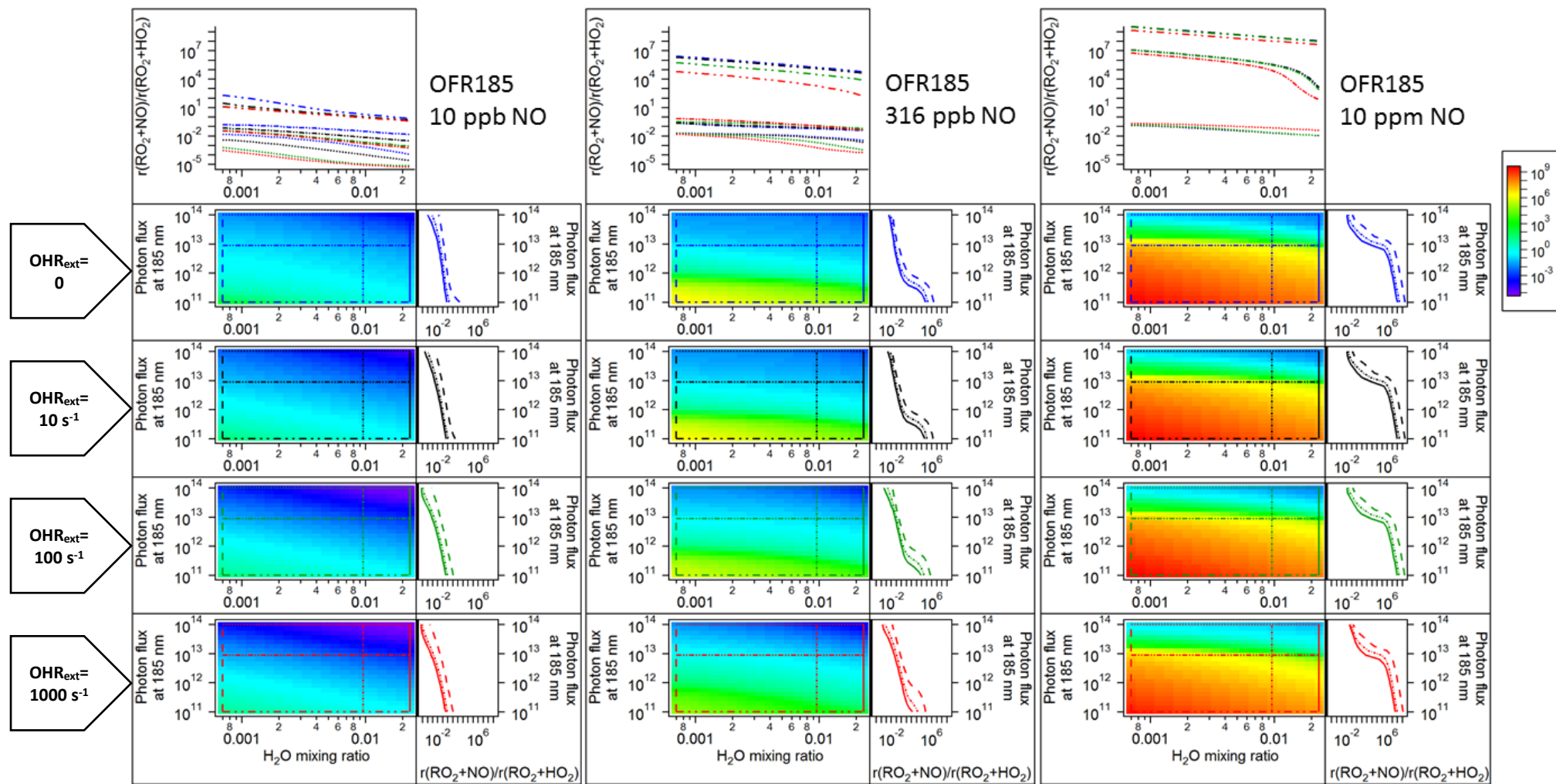
60
61

Ratio of OH exposure in the case with input NO to that in the corresponding case (same H₂O, UV, and OHR_{ext}) without input NO for OFR185-iNO



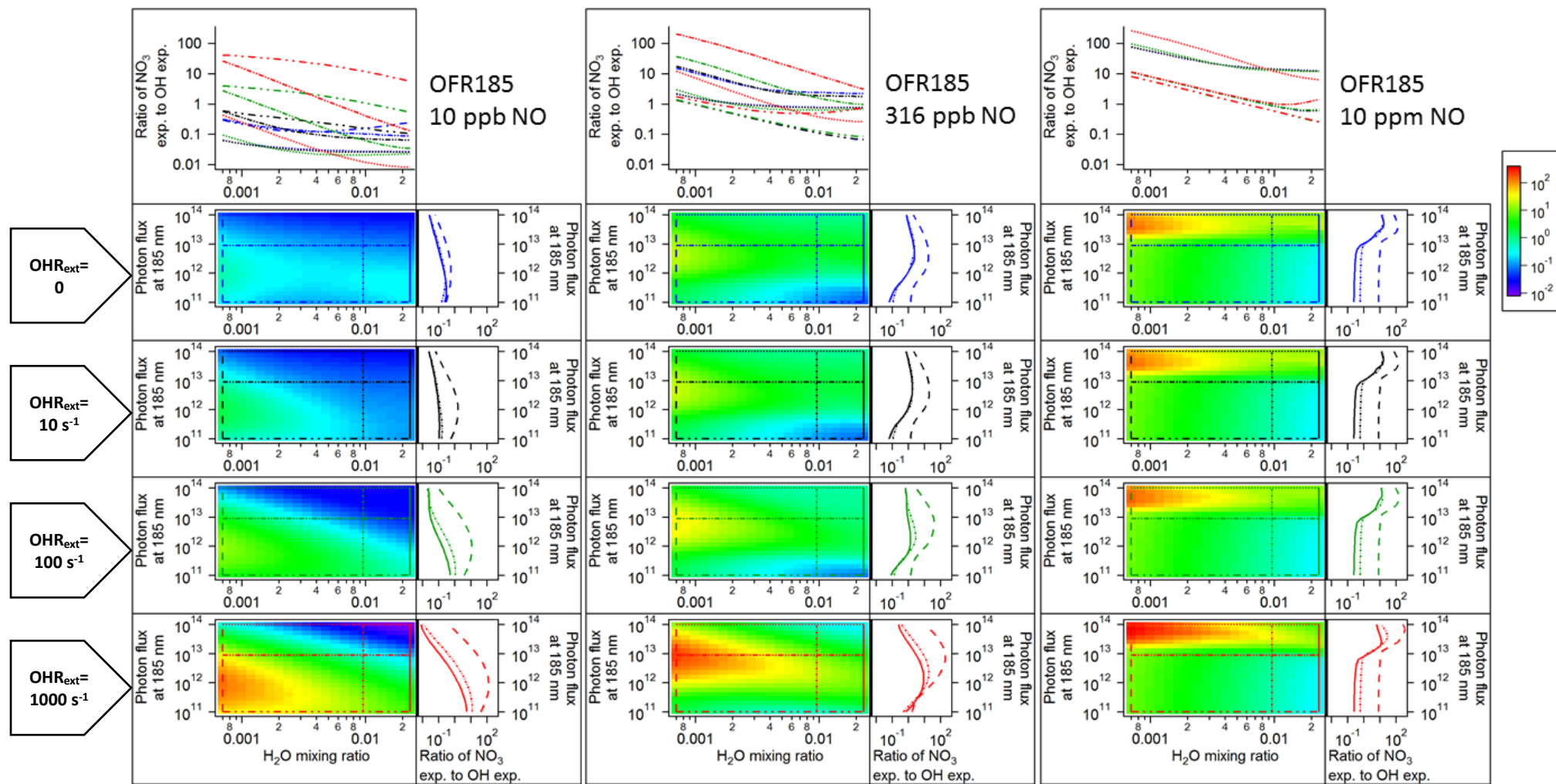
62
63

NO effective lifetime for OFR185-iNO

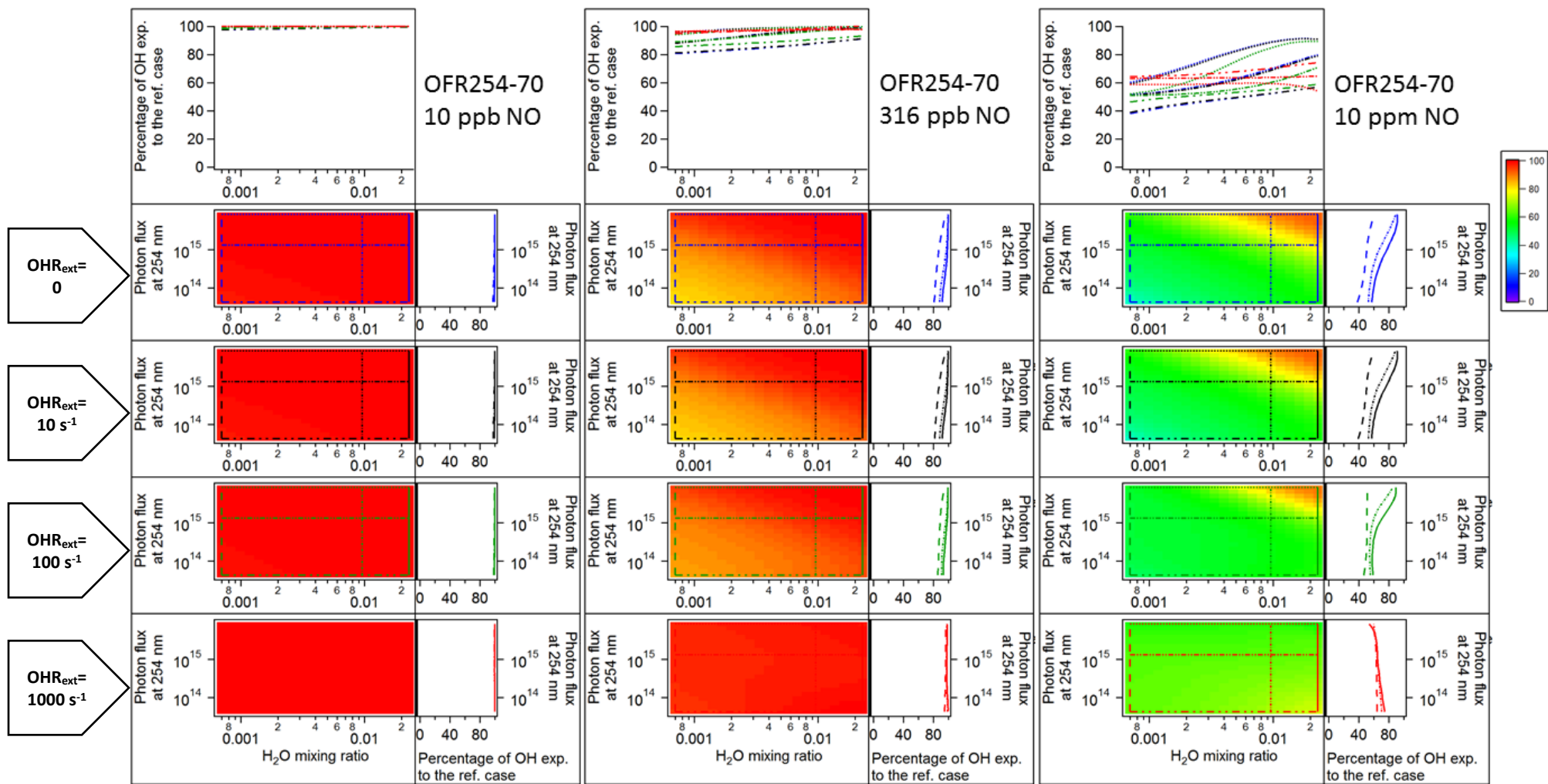


64
65

$r(\text{RO}_2+\text{NO})/r(\text{RO}_2+\text{HO}_2)$ for OFR185-iNO

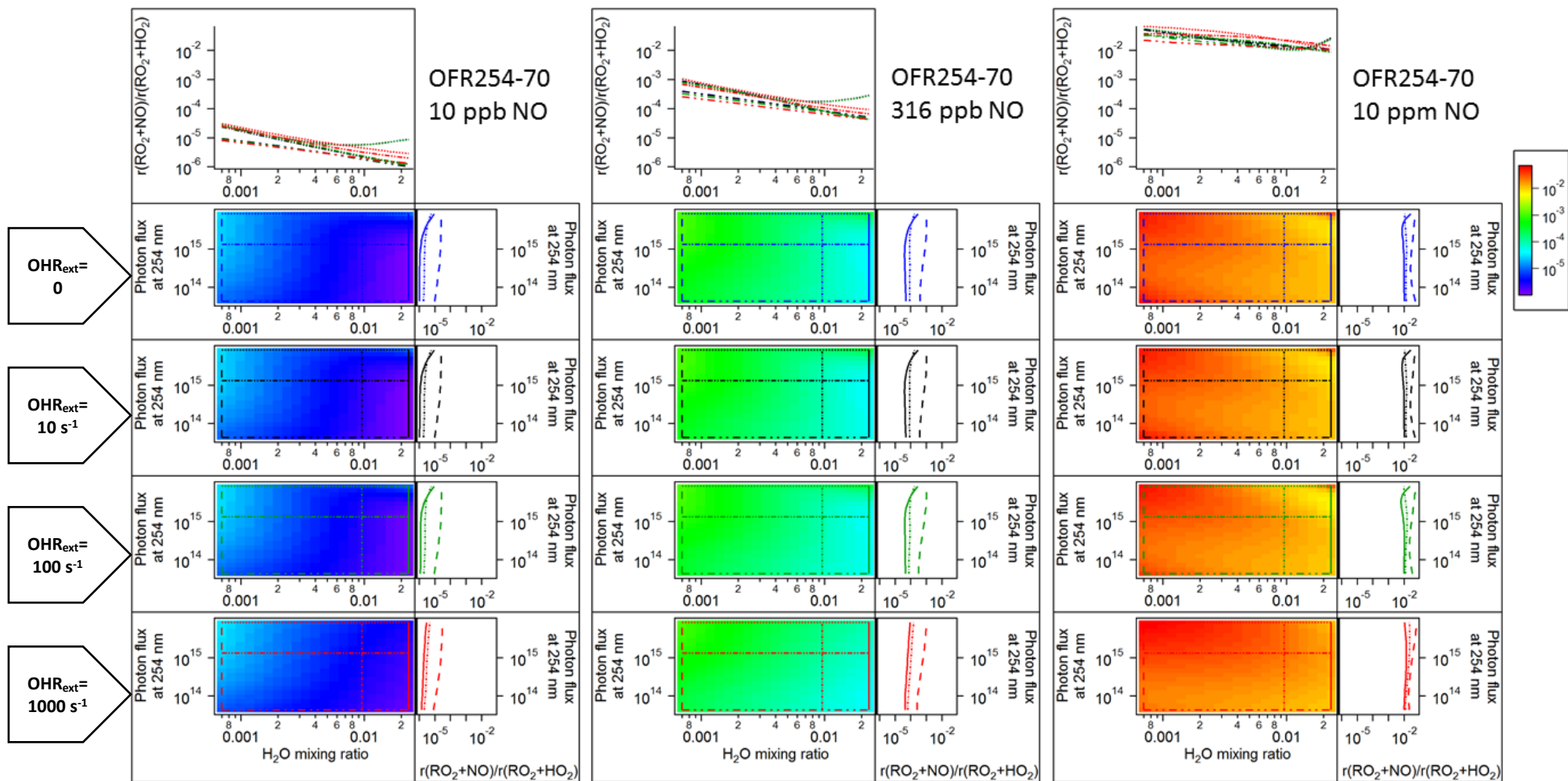


NO_3 exposure/OH exposure for OFR185-iNO



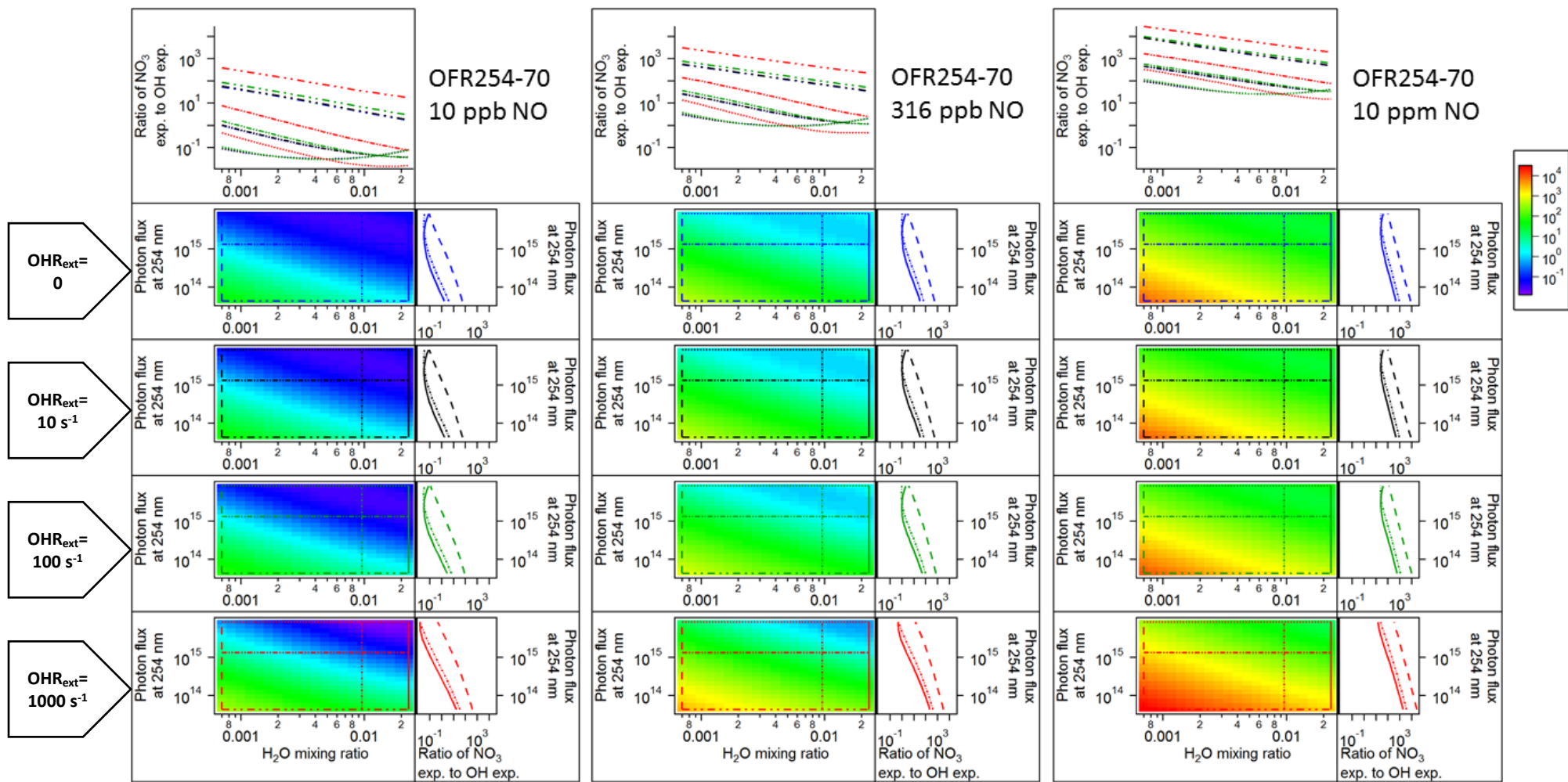
68
69

Ratio of OH exposure in the case with input NO to that in the corresponding case (same H₂O, UV, and OHR_{ext}) without input NO for OFR254-70-iNO



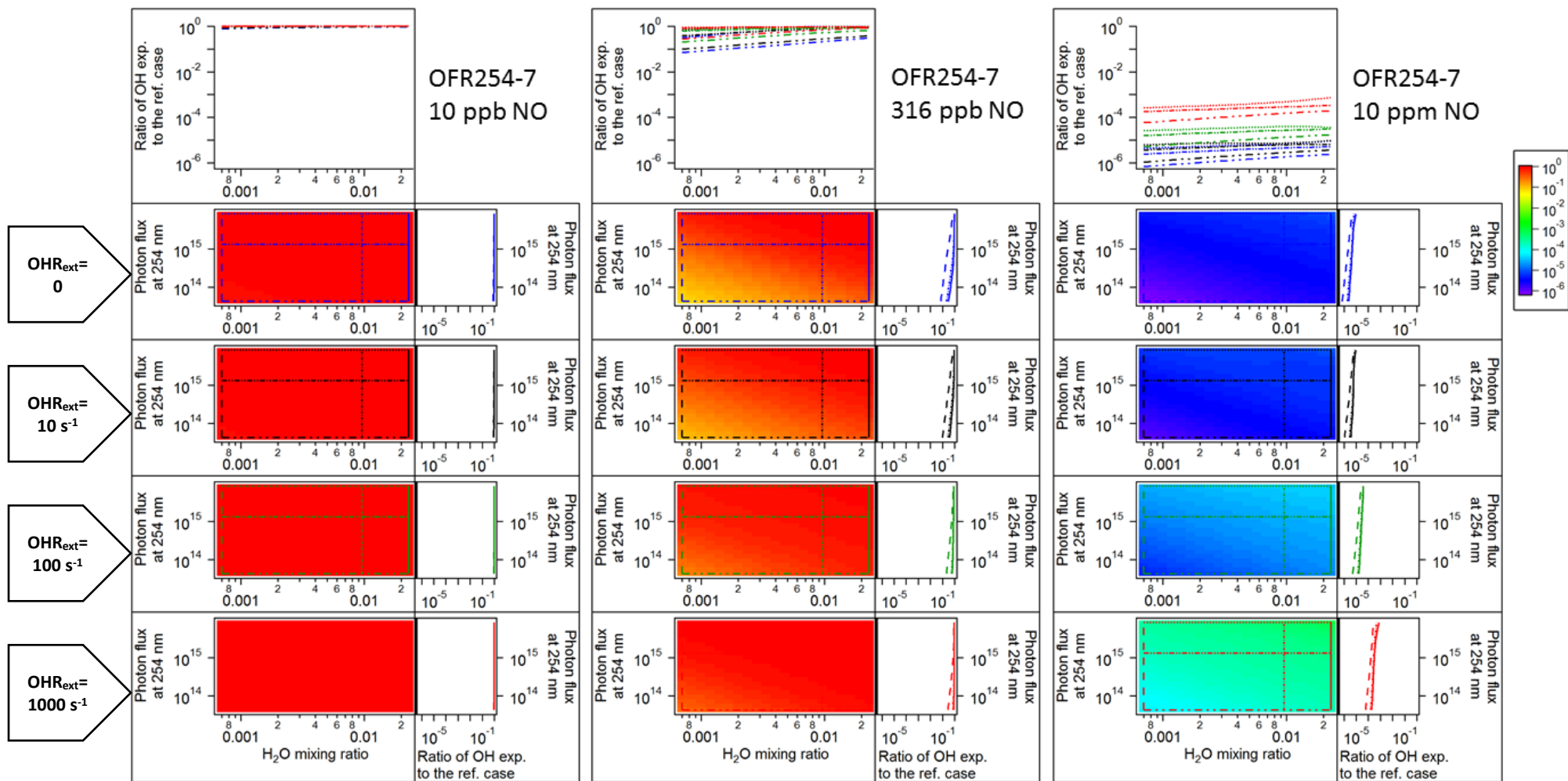
70
71

$r(\text{RO}_2+\text{NO})/r(\text{RO}_2+\text{HO}_2)$ for OFR254-70-iNO

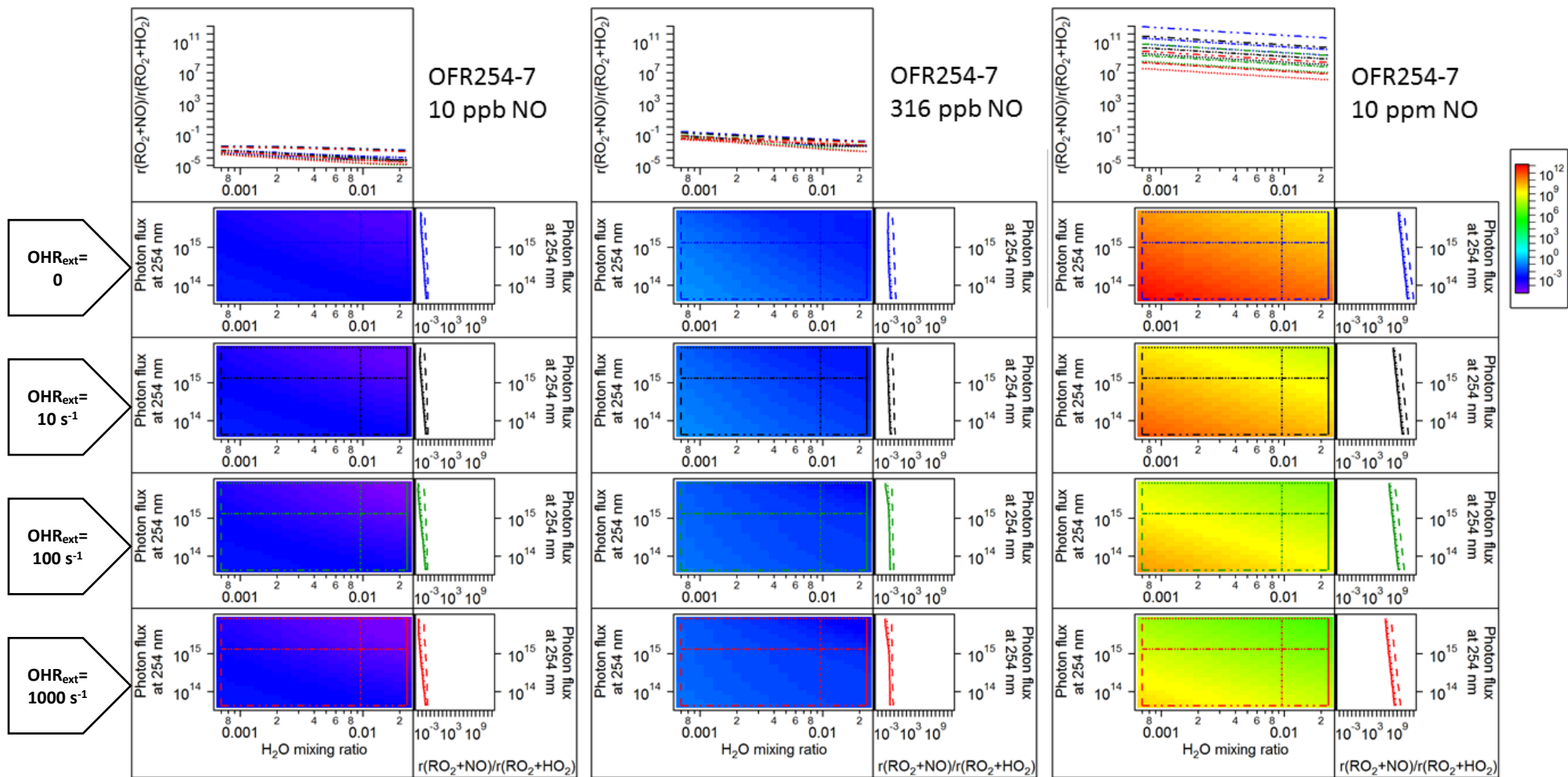


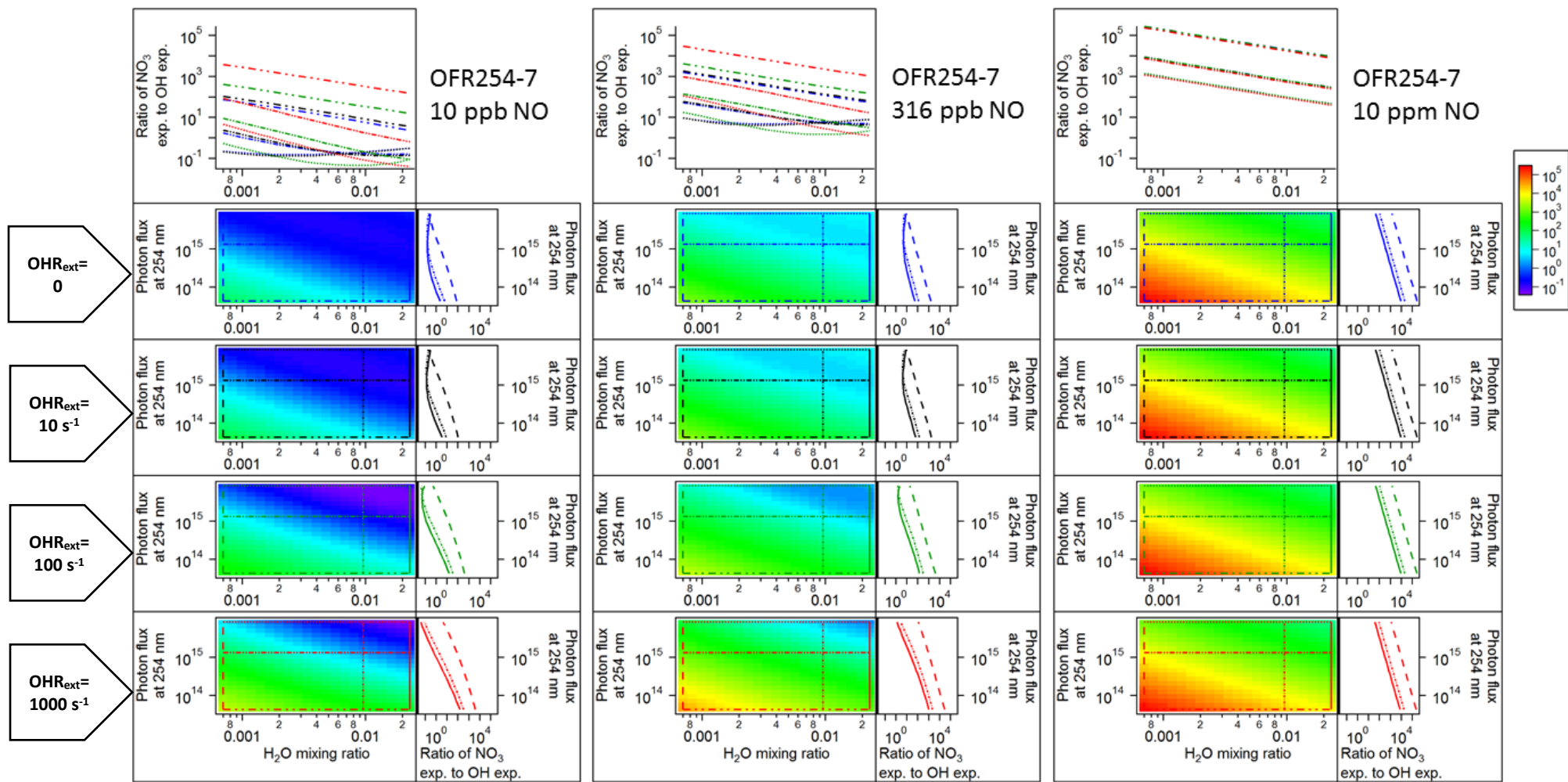
72
73

NO_3 exposure/OH exposure for OFR254-70-iNO



Ratio of OH exposure in the case with input NO to that in the corresponding case (same H₂O, UV, and OHR_{ext}) without input NO for OFR254-7-iNO





78
79

NO_3 exposure/OH exposure for OFR254-7-iNO

80 **Figure S7.** Dependence of several quantities in OFR185-iNO, OFR254-70-iNO, and OFR254-7-iNO on H₂O and UV, for OHR_{ext} of 0, 10, 100, and 1000 s⁻¹ (first, second, third, and
81 fourth row of image plots in each multi-panel composite, respectively). Each multi-panel composite shows a quantity for OFR185-iNO, OFR254-70-iNO, or OFR254-7-iNO. The
82 panels above and on the right of image plots are the line plots of the quantities shown in multi-panel composites in several typical cases. These cases are denoted in the image
83 plots by horizontal or vertical lines of the same color and pattern as in the line plots.
84 In detail, the cut lines are in blue, black, dark green, and red in the plots for the cases of 0, low, high, and very high (0, 10, 100, and 1000 s⁻¹, respectively) external OH reactivity,
85 respectively. Horizontal sparse-dash-dot-dot, dash-dot-dot, and dotted lines mark low, medium, and high water mixing ratios, respectively. Vertical dashed, dash-dot, and solid
86 lines mark low, medium, and high photon fluxes, respectively. Refer to Table 2 for more details on case labels. Each multi-panel composite has a color scale corresponding to its
87 image plots.

88 **S1. Rationale for selecting the criterion to quantify “high-NO” vs. “low-NO” conditions**

89 A “high-NO” condition results in more RO₂ reacted with NO than with HO₂. The amount of
90 RO₂ reacted with NO, r(RO₂+NO), is the integral of the rate of this reaction over the entire residence
91 time, i.e.,

92
$$r(\text{RO}_2+\text{NO}) = \int_0^{t_{res}} k(\text{RO}_2+\text{NO})[\text{RO}_2][\text{NO}]dt,$$

93 where t_{res} is residence time, $k(\text{RO}_2+\text{NO})$ is the rate constant of the reaction RO₂+NO, and [RO₂] and
94 [NO] are RO₂ and NO concentrations, respectively.

95 [RO₂] under a steady state approximation can be expressed as below

96
$$[\text{RO}_2] = \frac{\text{OHR}_{\text{VOC}}[\text{OH}]}{k(\text{RO}_2+\text{NO})[\text{NO}] + k(\text{RO}_2+\text{HO}_2)[\text{HO}_2] + k(\text{RO}_2+\text{RO}'_2)[\text{RO}'_2] + \dots},$$

97 where the numerator and denominator on the right side are respectively the RO₂ production rate
98 and its total first-order RO₂ loss rate constant. The production rate is simply the product of OH
99 concentration [OH] and OHR of VOC OHR_{VOC}. The total loss rate constant is the sum of those of all
100 RO₂ fates (RO₂+NO, RO₂+HO₂, RO₂+RO'₂,...).

101 We neglect all minor RO₂ fates. RO₂+RO'₂ is also neglected since RO₂+RO'₂ cannot compete
102 with RO₂+NO and RO₂+HO₂ for most RO₂ (Orlando and Tyndall, 2012), including under the typical
103 OFR conditions, and also to focus on the relative importance of RO₂+NO and RO₂+HO₂. As
104 $k(\text{RO}_2+\text{NO})$ and $k(\text{RO}_2+\text{HO}_2)$ are very similar (Orlando and Tyndall, 2012), we assume
105 $k(\text{RO}_2+\text{NO})=k(\text{RO}_2+\text{HO}_2)=k$. Then the [RO₂] estimation expression can be simplified as

106
$$[\text{RO}_2] \approx \frac{\text{OHR}_{\text{VOC}}[\text{OH}]}{k[\text{NO}] + k[\text{HO}_2]}.$$

107 Because OHR from VOC (including the reactivity of the products of the initial VOC(s)) is
108 relatively stable for most OFR experiments (Peng et al., 2015), OHR_{VOC} is assumed to be constant
109 here. Then r(RO₂+NO) can be rearranged as below

110
$$r(\text{RO}_2+\text{NO}) = \text{OHR}_{\text{VOC}} \int_0^{t_{res}} \frac{[\text{OH}][\text{NO}]}{[\text{NO}] + [\text{HO}_2]} dt.$$

111 Similarly, the amount of RO₂ reacted with HO₂, r(RO₂+HO₂), can be obtained

112
$$r(\text{RO}_2+\text{HO}_2) = \text{OHR}_{\text{VOC}} \int_0^{t_{res}} \frac{[\text{OH}][\text{HO}_2]}{[\text{NO}] + [\text{HO}_2]} dt.$$

113 Finally, we define “high-NO” conditions as those satisfying:

114
$$r(\text{RO}_2+\text{NO}) > r(\text{RO}_2+\text{HO}_2)$$

115 i.e.,

116
$$\frac{r(\text{RO}_2+\text{NO})}{r(\text{RO}_2+\text{HO}_2)} = \int_0^{t_{res}} \frac{[\text{OH}][\text{NO}]}{[\text{NO}] + [\text{HO}_2]} dt / \int_0^{t_{res}} \frac{[\text{OH}][\text{HO}_2]}{[\text{NO}] + [\text{HO}_2]} dt > 1$$

117 The ratio between the two integrals on the left side of the inequality can be calculated by the
118 model used in the present study. We thus take this inequality as the criterion for high-NO
119 conditions in this study.

120 **References**

121

122 Bishop, G. A. and Stedman, D. H.: Fuel Efficiency Automobile Test: Light-Duty Vehicles, [online] Available
123 from: http://www.feat.biochem.du.edu/light_duty_vehicles.html (Accessed 1 February 2017), 2013.

124 Karjalainen, P., Timonen, H., Saukko, E., Kuuluvainen, H., Saarikoski, S., Aakko-Saksa, P., Murtonen, T.,
125 Bloss, M., Dal Maso, M., Simonen, P., Ahlberg, E., Svenningsson, B., Brune, W. H., Hillamo, R., Keskinen,
126 J. and Rönkkö, T.: Time-resolved characterization of primary particle emissions and secondary particle
127 formation from a modern gasoline passenger car, *Atmos. Chem. Phys.*, 16(13), 8559–8570,
128 doi:10.5194/acp-16-8559-2016, 2016.

129 Orlando, J. J. and Tyndall, G. S.: Laboratory studies of organic peroxy radical chemistry: an overview with
130 emphasis on recent issues of atmospheric significance, *Chem. Soc. Rev.*, 41(19), 6294,
131 doi:10.1039/c2cs35166h, 2012.

132 Peng, Z., Day, D. A., Stark, H., Li, R., Lee-Taylor, J., Palm, B. B., Brune, W. H. and Jimenez, J. L.: HOx radical
133 chemistry in oxidation flow reactors with low-pressure mercury lamps systematically examined by
134 modeling, *Atmos. Meas. Tech.*, 8(11), 4863–4890, doi:10.5194/amt-8-4863-2015, 2015.

135